Theoretical Studies of the Photochemical Dynamics of Acetylacetone: Isomerzation, Dissociation, and Dehydration Reactions

Xue-Bo Chen,[†,‡] Wei-Hai Fang,*[,†] and David Lee Phillips*[,‡]

Department of Chemistry, Beijing Normal University, Beijing 100875, China, and Department of Chemistry, University of Hong Kong, Pokfulam Road, Hong Kong, China

Received: December 14, 2005; In Final Form: February 21, 2006

The potential energy surfaces of the C−O cleavage, rotational isomerization, keto−enolic tautomerization, and dehydration reactions of acetylacetone in the lowest triplet and ground states have been determined using the complete active space self-consistent field and density functional theory methods. The main photochemical mechanism obtained indicates that the acetylacetone molecule in the $S_2(^1\pi\pi^*)$ state can relax to the $T_1(^3\pi\pi^*)$ state via the S_2-S_1 vibronic interaction and an $S_1/T_1/T_2$ intersection. The C−O fission pathway is the predominant dissociation process in the $T_1(^3\pi\pi^*)$ state. Rotational isomerization reactions proceed difficultly in the ground state but very easily in the $T_1(^3\pi\pi^*)$ state. Keto−enolic tautomerization takes place with little probability for acetylacetone in the gas phase.

1. Introduction

The structure and reactivity of the acetylacetone (AcAc, $CH_3COCH_2COCH_3$) molecule have been important issues in many fields of science.[1−4] Particular attention has been devoted to (1) the structural characteristics of the tautomers, (2) the keto−enol tautomerization and UV-induced photoisomerization reactions, and (3) the photodissociation dynamics associated with this molecule. Although $CH_3COCH_2COCH_3$ is a prototype of β-diketones, it also belongs to the category of α,β-enone systems, due to the existence of an enolic form.[5−7] In principle, $CH_3COCH_2COCH_3$ may exist as an asymmetric (C_s) or symmetric (C_{2v}) structure in the ground state, and the asymmetric structure may interconvert via a hydrogen shift between the two oxygen atoms.[8−13] Recently, ultrafast electron diffraction experiments determined that the ground-state structure of AcAc has C_s symmetry.[14] There is an "abnormally" strong resonance-assisted hydrogen bond in the enolic form of AcAc, which is a model of the synergistic interplay between π delocalization and hydrogen-bond strengthening.[15,16] Dannenberg and Rios[17] demonstrated that the enolic form of AcAc was stabilized via a strong intramolecular hydrogen bonding in its cyclic conjugated system, of which the stabilization energy had been predicted to be 12.0 kcal/mol at the MP2/D95** level of theory. A value of 13.1 kcal/mol was determined for the stabilization energy by Gilli et al.,[18] which is much higher than the usual H-bond energy of 4 to ∼6 kcal/mol. In addition, electron delocalization and resonance in the enolic form considerably influences its reactivity. The structural complexity of AcAc makes its thermal and photochemical reactions become a challenging topic for both experimental and theoretical studies.

The keto−enol tautomerization has been investigated extensively by spectroscopic experiments[17,19−37] and theoretical calculations.[38,39] An electron diffraction experiment confirmed that the O···O distances in the gas-phase geometries of the keto and enol forms are 2.767 and 2.381 Å, respectively.[19] The equilibrium constants of the keto−enol tautomerism and the energy differences of two tautomers were examined by various techniques.[17,20,21] An equilibrium constant (k_{eq} = enol/keto) of 2.6 was obtained at 419 K from gas-phase NMR measurements.[22] An equilibrium constant of 9 was obtained at 373 K from gas-phase IR spectroscopy measurements,[23] and a constant of 32 was found at 290 K from an earlier electron diffraction study.[19] However, a UV spectroscopic study at 298 K did not detect absorption from the keto form,[24] which was further confirmed by X-ray photoelectron spectra at temperatures between 323 and 423 K.[25] All these data demonstrate that the enol form of AcAc is a stable isomer in the gas phase and the keto form may exist in solution.[26−31]

Intensive experimental studies[40−44] have been conducted to study the UV and IR photoisomerization of AcAc. It was observed that upon UV irradiation the intramolecular hydrogen bond was broken, leading to formation of nonchelated isomers.[40] Roubin and co-workers investigated the UV-induced isomerization reaction in xenon matrixes and observed infrared bands of at least three new species, which were assigned to be the CCT, TCC, and TCT isomers.[41,42] Nakata's group observed the isomers of CTC and TCT using low-temperature matrix-isolation infrared spectroscopy aided by DFT calculations.[43] Roubin revisited the photoisomerization reaction of AcAc and observed a back-conversion of nonchelated to chelated isomers. This back-conversion was only observed after laser irradiation at 230 nm and was not observed after annealing or IR irradiation.[44] Several recent experiments have examined the photodissociation dynamics of AcAc. UV and electron-impact spectroscopic studies showed a broad structureless absorption with a maximum at 266 nm, which is assigned to the first $\pi\pi^*$ transition of the enolic-acetylacetone (enolic-AcAc) species.[32,45] Upon 266 nm excitation, it is revealed that although AcAc is initially prepared in the $^1\pi\pi^*$ state, OH fragmentation is produced from the lowest $^3\pi\pi^*$ state,[46−50] with a time constant of 247 ± 43 ps.[50] Yoon et al. suggest that the upper bound for the dissociation energy of AcAc is estimated to be 90.3 kcal/mol, from the measured OH

* Corresponding authors. E-mail: Fangwh@bnu.edu.cn (W.-H.F.); Phillips@hkucc.hku.hk (D.L.P.).
† Beijing Normal University.
‡ University of Hong Kong.

10.1021/jp057306i CCC: $33.50
Published on Web 03/16/2006

product state distributions.[48] The exit barrier for the formation of the OH radical is assumed to be 16.0 kcal/mol.[49,51]

Although extensive investigations have been separately devoted to the nature of three aspects of AcAc,[1−3] much is still not resolved. We have made progress in better understanding the excited-state processes and reactions taking place in a range of related carbonyl-containing compounds[52] using the complete active space self-consistent field (CASSCF) and density functional theory (DFT) methods and we will use a similar approach here. In the present study, much effort has been put toward refining the simultaneous understanding of the mechanism(s) of formation of the OH fragment, photoinduced isomerization, and dehydration reactions. To gain more insight into the photochemistry and photophysics of photoinduced processes, we calculated the potential energy surface for the photodissociation of the C−O bond as well as the photoinduced isomerization and dehydration reactions at the CASSCF and DFT levels of theory.

2. Computational Details

Stationary structures for the enol form of AcAc in its five lowest electronic states (S_0, S_1, S_2, T_1, and T_2) and the keto form in its S_0, S_1, and T_1 states have been fully optimized by means of the CASSCF method. For comparison, the B3LYP procedure was used to determine stationary structures in the S_0 and T_1 states. All calculations were performed with the cc-pVDZ basis set. Once convergence is reached, the harmonic frequencies are examined at this point to confirm the geometry obtained to be a true minimum or first-order saddle point. The active space for the present CASSCF calculations is composed of 10 electrons in 8 orbitals, referred to as CAS(10,8). For the equilibrium geometries of the enolic form on the S_0, S_1, S_2, T_1, and T_2 states, the π and π^* orbitals of the C═O double bond, the C═C π and π^* orbitals, and the nonbonding orbitals of the two oxygen atoms should be included in the active space. In optimizing the structure of the transition state (TS) of the C−O bond cleavage, the C−O σ and σ^* orbitals are used as the active orbitals. A (10,8) active space is also employed in the calculations of the keto form. The lowest energy points of the surface crossings were determined by the state-averaged CASSCF optimization with the same (10,8) active space. All calculations were carried out using the Gaussian 98 program[53] package in either a Linux or Windows operating system.

3. Results and Discussion

The results of our theoretical study of AcAc will be discussed as follows. The AcAc geometric structures will be presented in section 3.1 for the ground state and in section 3.2 for the excited state. Section 3.3 will discuss the computation results for the adiabatic excitation energy. The isomerization reactions will be discussed in section 3.4, including the rotational isomerization of enolic-AcAc and the keto−enolic tautomerization. In section 3.5, the dehydration reaction will be examined. The formation pathway of the OH product is also described for the S_0 and T_1 states in section 3.6.

3.1. Geometric Structures of Enol and Keto Forms in the Ground State. The C_s structure of enolic-AcAc in the ground state was confirmed to be a global minimum at the CAS(10,8) and B3LYP levels of theory. This structure is referred to as E-S_0 (where E stands for enolic-AcAc) and is depicted in Figure 1 with selected bond parameters and an atom-labeling scheme. The geometric structure of E-S_0 is an open six-membered ring where the lengths of the C2−O3, C7−C10, C2═C7, and C10═O11 bonds are 1.334, 1.475, 1.354, and 1.215 Å, respectively, at the CAS(10,8)/cc-pVDZ level of theory. This result clearly indicates that enolic-AcAc exhibits some π-delocalization character, leading to shorter C2−O3, C7−C10 and longer C═C, C═O bonds compared to the normal distances typically found in enols.[15,16] The O3···O11 distance is confirmed to be 2.512 Å at the B3LYP/cc-pVDZ level of theory, and this value agrees well with those previously reported by an electron diffraction experiment at room temperature (2.512 Å[54]) and X-ray crystallography experiments (2.535 and 2.547 Å[55,56]). To clarify the controversy about the enol structures of AcAc in the ground state,[19,54] we optimized the C_{2v} structure at the B3LYP and the CAS(10,8) levels of theory, respectively. These results show that the C_{2v} structure in the ground state is the first-order saddle point, which connects the two equivalent minima of E-S_0. The present calculation results provide support that the C_{2v} structure is less stable than the C_s structure by 1.7 kcal/mol, which agrees with Nagashima et al.'s energy order from the results of B3LYP calculations.[43] This suggests that the two equivalent C_s minimum structures of AcAc (O3−H8···O11 and O3···H8−O11) may interconvert via the transition state of the C_{2v} structure with very low barrier.

When the O−H, CH_3CO, and CH_3COH groups rotate around the C2−O3, C7−C10, and C2−C7 bonds of E-S_0, respectively, and these rotations are proceeded in turn, seven more conformers were obtained, namely, CCT(S_0), TCC(S_0), CTC(S_0), TCT(S_0), CTT(S_0), TTC(S_0), and TTT(S_0), according to the relative position (T for trans and C for cis). The seven conformers have been confirmed to be minima by CAS(10,8) and B3LYP calculations. The detailed computational results are given in the Supporting Information, and the relative energies of the eight isomers have been summarized in Table 1. Similar to the geometric structure of E-S_0, the seven isomers in the ground state also exhibit C_s symmetry. The order of relative energies is E(S_0) < TCT(S_0) < CTT(S_0) < CTC(S_0) < TCC(S_0) < TTC(S_0) < TTT(S_0) < CCT(S_0) at the CAS(10,8) level of theory, which differs somewhat from the results of the B3LYP calculations.

The distance of O11···H8 is 1.890 Å in E-S_0 where the strong intramolecular hydrogen bond was found. But there is no hydrogen bonding between H8 and O11 in the structure of CCT(S_0). So, the energy difference between E-S_0 and CCT(S_0) is considered to be the stabilization energy of the hydrogen bond in E-S_0. The stabilization energy of the H-bond has been determined to be 12.1 kcal/mol at the CAS(10,8) level of theory. This is in agreement with values previously reported to be 12.0 and 13.1 kcal/mol (refs 17 and 18).

The ground-state geometric structure of AcAc for the keto form (denoted here as K-S_0 where K stands for keto) has also been determined by both B3LYP and CAS(10,8) calculations, and the optimized geometry is depicted in Figure 1. The K-S_0 minimum has a C_2 symmetry structure. In comparison with structures previously reported,[14,19] the present calculations have a relatively large O3···O11 distance, which was determined to be respectively 4.1 and 4.0 Å at the CAS(10,8) and B3LYP levels of theory. The keto form of AcAc is less stable than the enolic form by 6.8 kcal/mol at the B3LYP level of theory with the zero-point correction included, and this value is close to the experimental value of 8.3 kcal/mol.[31,32,58] E-S_0 is a global minimum in the potential energy surface of the ground state, and it is considered to be the starting reactant for the C2−O3 fission process as well as for the photoinduced isomerization and dehydration reactions.

3.2. Geometric Structures of Enol and Keto Forms in the Excited States. The geometric structures of the enolic form in

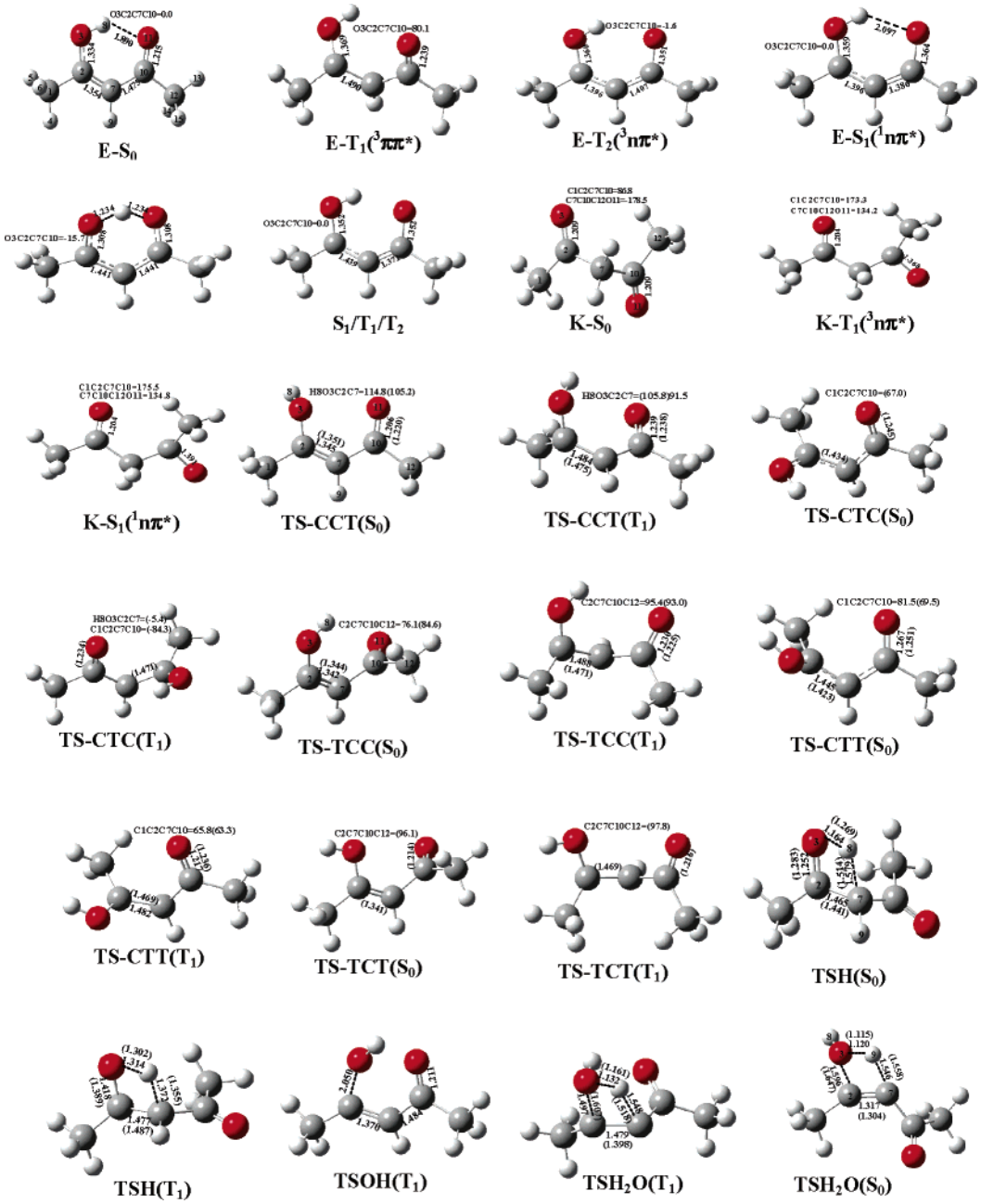

Figure 1. Schematic structures of stationary and intersection points in the lowest five electronic states of AcAc, along with the atom-labeling scheme in the S_0 structures and the selected bond parameters at the levels of CAS(10,8)/cc-pVDZ and B3LYP/cc-pVDZ (in parentheses).

TABLE 1: Relative Energies for Isomers in the S_0 and T_1 States at the CAS(10,8)/cc-pVDZ and B3LYP/cc-pVDZ (the Values in Parentheses) Levels

species	relative energy	species	relative energy
E-S_0	0.0(0.0)	CCT(S_0)	12.1(17.2)
CTC(S_0)	6.8(11.8)	CTT(S_0)	6.7(12.9)
TCC(S_0)	8.4(14.3)	TCT(S_0)	2.3(15.5)
TTC(S_0)	8.4(16.7)	TTT(S_0)	11.7(19.3)
E-T_1	56.7(68.0)	CCT(T_1)	58.4(73.8)
CTC(T_1)	(72.8)	CTT(T_1)	58.3(73.2)
TCC(T_1)	58.7(72.7)	TCT(T_1)	(73.7)

the T_1, T_2, S_1, and S_2 states have been characterized by the CAS(10,8) calculations. These structures are labeled, respectively, as E-T_1, E-T_2, E-S_1, and E-S_2 and are depicted in Figure 1. The T_1 state of the enolic form of AcAc is assigned to be a C=C $\pi \rightarrow \pi^*$ transition based on an analysis of the molecular orbitals and their populations. The length of the C2−C7 bond is elongated to 1.490 Å at the CAS(10,8) level of theory, compared to 1.354 Å in the E-S_0 minimum at the same level of theory. The $\pi \rightarrow \pi^*$ excitation leads to a nonplanar and non-hydrogen-bonded E-T_1 minimum in which the distance of O11···H8 is 2.729 Å and the dihedral angle of O3−C2−C7−C10 is 80.1° at the CAS(10,8) level of theory. Meanwhile, the conformers of TCT, CTT, CTC, CCT, and TCC in the $T_1(^3\pi\pi^*)$ state have also been determined by the CAS(10,8) and B3LYP calculations, and these structures are depicted in the Supporting Information. Similar to the geometric structures of E-T_1, the TCT(T_1), CTT(T_1), CTC(T_1), CCT(T_1), and TCC(T_1) minima exhibit nonplanar structures and have an elongated C2−C7 bond length compared to that of the corresponding values in the S_0 minima. These isomers also originate from the C=C $\pi \rightarrow \pi^*$ transition, which is responsible for the changes in their structures. In comparison with the E-T_1 minimum structure, the differences in the structures of the conformers comes from the rotation of the CH_3-

CO, CH_3COH, and O−H moieties. As listed in Table 1, there were slight differences in energy among the isomers of the T_1 sate.

The CAS(10,8) calculations confirmed that the E-T_2 minimum originated from an n → π^* excitation, where one electron is promoted from the O11 nonbonding orbital to the C10═C11 π^* orbital. The length of the C10−O11 bond in the E-T_2 structure is elongated to 1.351 Å at the CAS(10,8) level of theory and exhibits some single-bond character. The geometric structure of E-T_2 is nearly planar with the O3−C2−C7−C10 dihedral angle of −1.6° at the CAS(10,8) level of theory. The π electrons located in the C2−C7 bond in the ground state of enolic-AcAc are delocalized to the region of the C2−C7−C10 moiety in the E-T_2 minimum structure. Similar to E-T_2, the E-S_1 also originates from the n → π^* transition. Like the geometric structure of E-S_0, the E-$S_1(^1n\pi^*)$ minimum has a C_s symmetry structure, where the H4, H8, H9, H13, and all heavy atoms are coplanar. The distance of H8···O11 was found to be 2.097 Å, which shows that the planar S_1 minimum is a weak hydrogen-bonded structure. Upadhyaya et al.[49] reported a CIS calculation of the $S_2(\pi\pi^*)$ geometric structure for enolic-AcAc, and a C_{2v} structure was predicted to be minimum on the S_2 surface of enolic-AcAc. We reoptimize the S_2 structure of the enol form at the CAS(10,8) level, as shown in Figure 1. With respect to the E-S_0 minimum, the bond length of C2−C7 in the S_2 structure is elongated to 1.441 Å and the bond length of C7−C10 is slightly shortened.

The lowest triplet and singlet excited states for the keto form have also been optimized by the CAS(10,8) calculations, and these structures are referred to as K-T_1 and K-S_1, respectively. The K-T_1 state originates from the n → π^* excitation where one electron is promoted from the O11 nonbonding orbital to the C10═O11 π^* orbital. In comparison with the geometric structure of K-S_0, the C10−O11 bond is elongated, which is accompanied with the formation of a pyramidal acetyl group. The K-S_1 structure also originates from the n → π^* transition, which has been plotted in Figure 1.

3.3. Adiabatic Excitation Energies. The electronic structures and spectra of AcAc were measured by Nakanishi et al.[32] The relatively strong bands observed at 38 020 and 56 800 cm^{-1} for the enol form were assigned to the first and second $\pi\pi^*$ excitations, respectively.[32] Various spectral techniques have further confirmed that the relatively strong band with a peak at around 266 nm (37 594 cm^{-1}) is assigned to be the first $\pi\pi^*$ transition of the enolic form.[46−49] Walzl et al. reported electron-impact spectra for various diketone compounds.[45] It was established that the $^1\pi\pi^*$ excitation in the enolic form of AcAc was 4.70 eV (37 907 cm^{-1}), and the first spin-allowed and spin-forbidden n → π^* transitions were determined to be 4.04 eV (32 584 cm^{-1}) and 3.57 eV (28 793 cm^{-1}), respectively.

The adiabatic excitation energies from E-S_0 to E-$S_1(^1n\pi^*)$ and E-T_2 ($^3n\pi^*$) were determined to be 3.68 and 3.34 eV, respectively, by the present CAS(10,8) calculations, which is, respectively, 0.36 and 0.23 eV lower than the vertical excitation energies.[45] The CAS(10,8) calculations give a value of 56.7 kcal/mol for the E-S_0 → E-$T_1(^3\pi\pi^*)$ transition, and this agrees well with the value of 56.0 kcal/mol reported previously.[49] With respect to the zero point of the ground state, the position of E-$S_2(^1\pi\pi^*)$ in energy is 106.5 kcal/mol at the CAS(10,8) level of theory with the zero-point correction included. Experimentally, it was well established that the vertical excitation energy is around 108.4 kcal/mol from the ground state to the E-S_2-$(^1\pi\pi^*)$ state. In comparison to the experimental findings, the present calculations provide a reasonable description of the adiabatic excitation energies from E-S_0 to E-$S_1(^1n\pi^*)$, E-T_1-$(^3\pi\pi^*)$, and E-T_2 ($^3n\pi^*$), but the adiabatic excitation energy from E-S_0 to E-$S_2(^1\pi\pi^*)$ may be overestimated by a few kcal/mol.

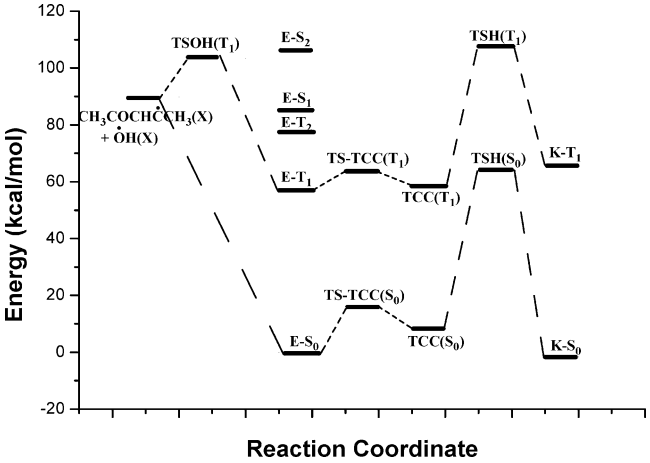

Figure 2. Schematic potential energy surfaces for the C2−O3 fission and keto−enolic tautomerization reactions in the S_0 and the T_1 ($^3\pi\pi^*$) states along with the CAS(10,8)/cc-pVDZ-computed relative energies (kcal/mol).

3.4. Isomerization Reactions. *3.4.1. Rotational Isomerization Reactions.* The O−H, CH_3COH, and CH_3CO groups of E-S_0 rotate around the C2−O3, C2−C7, and C7−C10 axes, leading to the isomers of CCT(S_0), CTC(S_0), and TCC(S_0), respectively. A transition state was found and is referred to as TS-TCC(S_0) in Figure 1. TS-TCC(S_0) has been confirmed to connect the E-S_0 and TCC(S_0) by the IRC calculations at the B3LYP level of theory. The dihedral angle of C2−C7−C10−C12 in TS-TCC-(S_0) was determined to be 84.6° and 76.1° at the B3LYP and CAS(10,8) levels of theory, respectively, while it is 180.0° in E-S_0 and 0.0° in TCC(S_0). With respect to the E-S_0 minimum, the barrier height to the rotational isomerization is 16.2 kcal/mol at the CAS(10,8) level of theory with the zero-point correction included, and the value changed to 21.7 kcal/mol at the B3LYP level of theory with the zero-point correction included. Similar rotational isomerization processes from E-S_0 to CCT(S_0) and CTC(S_0) have been investigated at the B3LYP level of theory. The barrier heights were determined to be 21.2 and 55.2 kcal/mol, respectively. Structures of the related transition states and potential energy profiles for the rotational isomerization processes are plotted in Figures 1 and 2, respectively.

The two-step process for formation of CTT(S_0) is depicted in Scheme 1. Transition states of TS-CCT(S_0) and TS-CTT(S_0) have been determined by CAS(10,8) and B3LYP computations. In the first step, the O−H rotation around the C2−O3 bond leads to the dihedral angle of H8−O3−C2−C7 increasing from 0° in E-S_0 to about 110° in TS-CCT(S_0) and 180° in CCT(S_0). In the second step, the rotation of the CH_3COH group is accompanied by the dihedral angle of C1−C2−C7−C10 decreasing from 180° in CCT(S_0) to about 75° in TS-CTT(S_0), and then it goes to 0.0° in CTT(S_0). The barrier height in the second step from CCT(S_0) to CTT(S_0) is determined to be 46.6 and 45.5 kcal/mol by the B3LYP and CAS(10,8) calculations, respectively. In the rotational process of the CH_3COH group, the C2═C7 π bond is broken, which is responsible for a high barrier on the pathway. As described in Scheme 2, the TCT-(S_0) isomer can be formed via a two-step process with a barrier of 21.2 kcal/mol in the first step. Since rotational isomerization processes in E-S_0 involve a breakage of the intramolecular

SCHEME 1

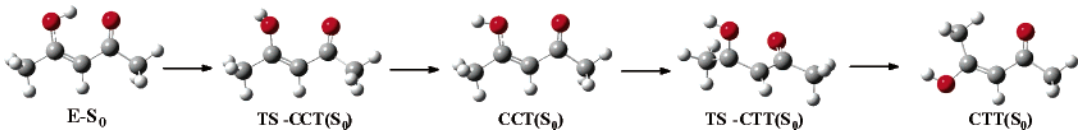

SCHEME 2

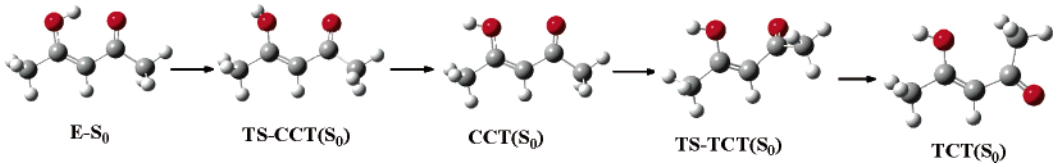

TABLE 2: Barrier Height (kcal/mol) for Rotational Isomerization in the S_0 and T_1 States at the CAS(10,8)/cc-pVDZ and B3LYP/cc-pVDZ (the Values in Parentheses) Levels

items	transition state	barrier height
O−H rotation for E-S_0	TS-CCT (S_0)	16.8(21.2)
CH_3COH rotation for E-S_0	TS-CTC(S_0)	(55.2)
CH_3CO rotation for E-S_0	TS-TCC(S_0)	16.2(21.7)
CH_3COH rotation for CCT(S_0)	TS-CTT(S_0)	45.5(46.6)
CH_3CO rotation for CCT(S_0)	TS-TCT(S_0)	(5.7)
O−H rotation for E-T_1	TS-CCT(T_1)	1.9(6.3)
CH_3COH rotation for E-T_1	TS-CTC(T_1)	(5.1)
CH_3CO rotation for E-T_1	TS-TCC(T_1)	6.9(12.0)
CH_3COH rotation for CCT(T_1)	TS-CTT(T_1)	0.1(0.6)
CH_3CO rotation for CCT(T_1)	TS-TCT(T_1)	(10.1)

O−H···O hydrogen bond or breaking the C=C π bond, these processes do not proceed easily in the ground state.

The same theoretical approaches were employed to deal with the rotational isomerization processes in the T_1 state. The geometric structures of the transition state are shown in Figure 1, and the barrier heights are presented in Table 2. As pointed out before, the T_1 state of enolic AcAc originates from the $\pi \rightarrow \pi^*$ transition of the C=C double bond. The C2−C7 bond exhibits single-bond character in the E-T_1 structure, and the CH_3-COH moiety rotates about 80° with respect to the E-S_0 structure. As a result of these, the intramolecular O−H···O hydrogen bond does not exist in E-T_1, and the O−H, CH_3COH, and CH_3CO groups can rotate around the C−C or C−O single bond freely. It is reasonable to expect that the rotational isomerization reactions take place more easily in the T_1 state than in the S_0 state, which is confirmed by the calculated barrier heights on the T_1 pathways.

The B3LYP calculations predict that the barrier heights are 6.3, 5.1, and 12.0 kcal/mol for the isomerization processes from E-T_1 to CCT(T_1), CTC(T_1), and TCC(T_1), respectively. Similar to formation of CTT(S_0) and TCT(S_0) in the ground state, the CTT(T_1) and TCT(T_1) isomers can be produced by the two-step processes of E-T_1 → TS-CCT(T_1) → CCT(T_1) → TS-CTT-(T_1) → CTT(T_1) and E-T_1 → TS-CCT(T_1) → CCT(T_1) → TS-TCT(T_1) → TCT(T_1), respectively. There is nearly no barrier for formation of CTT(T_1) from CCT(T_1), while the barrier height is about 10 kcal/mol on the second step from CCT(T_1) to TCT-(T_1). The calculated barrier heights reveal that E-T_1, CCT(T_1), and CTC(T_1) are the predominant isomers in the T_1 state of enolic AcAc.

3.4.2. Keto-Enol Tautomerization. We attempted to optimize a cis-keto structure of AcAc with C_s symmetry. But the obtained structure was confirmed to the second-order saddle point by frequency calculations. Starting from the initial cis-keto structure, the B3LYP optimization was performed without any symmetry constraint, which leads to formation of the trans-keto structure in Figure 1. The present calculations reveal that no cis-keto minimum exists for AcAc in the gas phase. The UV spectroscopic study at 298 K did not detect absorption from the cis-keto form,[24] which was further confirmed by X-ray photoelectron spectra at temperatures between 323 and 423 K.[25] The cis-keto form was suggested to exist in solution.[26−31]

It can be seen from the structures of E-S_0 and K-S_0 in Figure 1 that keto−enol tautomerization involves rotational isomerization and hydrogen transfer. The first step is a rotation of the CH_3CO group around the C10−C7 bond to produce the TCC-(S_0) isomer, which has been discussed in section 3.4.1. The second step can take place via a four-centered transition state, TSH(S_0), which involves the H8 transfers from O3 to C7. The IRC calculations at the B3LYP level confirmed that TSH(S_0) is the transition state that connects TCC(S_0) and K-S_0. With respect to the E-S_0 minimum, the position of TSH(S_0) in energy is, respectively, 63.9 and 61.9 kcal/mol at the CAS(10,8) and B3LYP levels of theory with the zero-point correction included. The high barrier in the rate-determining step indicates that the keto−enol tautomerization in the ground state takes place with little probability. Direct keto−enolic tautomerization reaction has been studied for malonaldehyde ($HCOCH_2COH$).[59] The barrier height was determined to be 59.99 kcal/mol, which is close to that for AcAc ($CH_3COCH_2COCH_3$). Since the reaction involves a highly strained four-centered transition state, which leads to a very high barrier, the direct keto−enolic tautomerization proceeds very difficultly for $CH_3COCH_2COCH_3$ and $HCOCH_2COH$ in the gas phase. In aqueous solution, however, water molecules function as a relay and enable the tautomerization reaction to proceed easily. DFT calculations indicated that the keto−enolic tautomerization proceeded by a small barrier due to the enhanced reactivity of water hydrogen-bonded networks.[59]

The same two-step mechanism was found for the keto−enolic tautomerization in the lowest triplet state, which can be represented as E-T_1 → TS-TCC(T_1) → TCC(T_1) → TSH(T_1) → K-T_1. The IRC calculations at the B3LYP level confirm that TSH(T_1) connects the corresponding reactant and product. As depicted in Figure 1, the bond parameters for the four-centered transition state, TSH(T_1), differs from those of TSH(S_0). The distance of H8−C7 is shortened from 1.514 Å in TSH(S_0) to 1.355 Å in TSH(T_1) at the B3LYP level of theory. With respect to the zero level of the TCC(T_1) minimum, the barrier height was determined to be 31.4 kcal/mol at the B3LYP level of theory with the zero-point correction included. The relatively high barrier indicates that the keto−enol tautomerization in the triplet state takes place difficultly.

3.5. Dehydration Reaction. As shown in Figure 3, the dehydration reaction of E-S_0 is a three-step process: E-S_0 → TS-CCT(S_0) → CCT(S_0) → TS-CTT(S_0) → CTT(S_0) → TSH_2O-

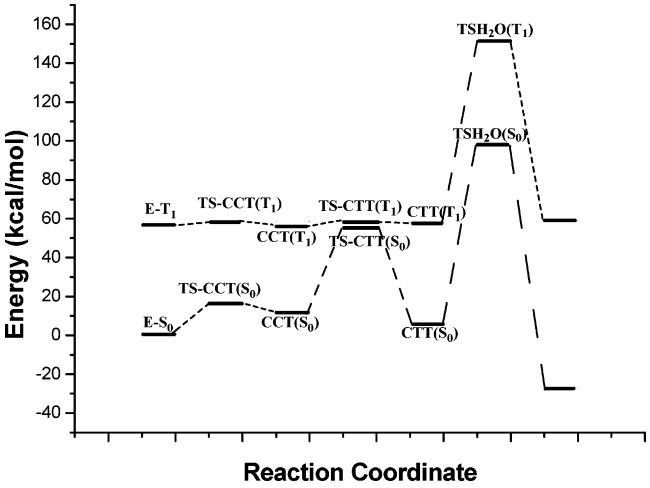

Figure 3. Schematic potential energy surfaces for the dehydration reaction in the S_0 and the $T_1(^3\pi\pi^*)$ states along with the CAS(10,8)/cc-pVDZ-computed relative energies (kcal/mol).

(S_0) → $CH_3C{\equiv}CCOCH_3(\tilde{X})$ + $H_2O(\tilde{X})$. We found a four-centered transition state on the S_0 potential energy surface by the B3LYP and CAS(10,8) calculations. The transition state is referred to as $TSH_2O(S_0)$ and is depicted in Figure 1. The IRC calculations at the B3LYP level of theory gave evidence that $TSH_2O(S_0)$ connected the $CTT(S_0)$ in the direction of the reactant and $CH_3C{\equiv}CCOCH_3(\tilde{X})$ + $H_2O(\tilde{X})$ in the direction of the product. With respect to the E-S_0 minimum, $TSH_2O(S_0)$ has an energy of 89.6 kcal/mol at the B3LYP level of theory with the zero-point correction included. The calculated barrier height predicts that the dehydration reaction of E-S_0 does not take place under normal condition.

Like the dehydration reaction in the ground state, the three-step mechanism has also been determined in the T_1 state, which is represented as E-T_1 → TS-CCT(T_1) → CCT(T_1) → TS-CTT(T_1) → CTT(T_1) → $TSH_2O(T_1)$ → $CH_3C{=}CCOCH_3(^3\pi\pi^*)$ + $H_2O(\tilde{X})$. As depicted in Figure 1, the structure of $TSH_2O(T_1)$ is similar to that of $TSH_2O(S_0)$. The main difference between the two structures is associated with the distance of the C2−C7 bond, which is 1.479 Å in $TSH_2O(T_1)$ and 1.317 Å in $TSH_2O(S_0)$ at the CAS (10,8) level of theory. This structural difference in the transition state provides a clue that $TSH_2O(S_0)$ leads to formation of $CH_3C{\equiv}CCOCH_3(\tilde{X})$ in the ground state, while $TSH_2O(T_1)$ is correlated with the triplet-state product of $CH_3C{=}CCOCH_3(^3\pi\pi^*)$. The energy gap between $CH_3C{\equiv}CCOCH_3(\tilde{X})$ and $CH_3C{=}CCOCH_3(^3\pi\pi^*)$ has been determined to be 86.5 kcal/mol by the CAS(10,8) calculations with the zero-point correction included. With respect to the zero level of E-S_0, the position of $TSH_2O(T_1)$ in energy was determined to be 142.3 kcal/mol at the B3LYP level of theory. This predicts that the dehydration reaction in the T_1 state does not take place even with excitation at a wavelength of 193 nm. The dehydration reaction along the S_1 pathway leads to products in an excited singlet state. In addition, the dehydration reaction involves a breakage of the C−O and C−H bonds and formation of the O−H σ and C−C π bonds simultaneously. One can expect that the barrier to the S_1 dehydration is much higher than that on the T_1 pathway. Thus, the S_1 pathway for $CH_3COCH_2COCH_3$ dehydration is not optimized in the present work.

3.6. Formation of the OH Radicals. The OH radical has been observed as one of the main products after UV irradiation of enolic-AcAc in several experiments.[46−49] We attempted to optimize a transition state for the C2−O3 fission in the ground state, but our efforts led to the dissociation limit of $CH_3COCHCCH_3(\tilde{X}^2A)$ + $OH(\tilde{X}^2\Pi)$. This suggests that no potential barrier exists above endothermicity on the S_0 pathway. The C2−O3 cleavage was predicted to be endothermic by 89.8 kcal/mol by supermolecular optimization at the CAS(10,8) level of theory with the zero-point correction included. The dissociation energy for the C2−O3 bond cleavage has been estimated to be 90.3 kcal/mol from the measured OH product state distributions.[48]

A transition state for the C2−O3 scission on the $T_1(^3\pi\pi^*)$ potential energy surface, referred to as $TSOH(T_1)$, has been determined by the CAS(10,8) calculations. As shown in Figure 2, the $TSOH(T_1)$ transition state connects the $CH_3COCHCCH_3(\tilde{X}^2A)$ + $OH(\tilde{X}^2\Pi)$ products and the E-$T_1(^3\pi\pi^*)$ minimum. This was confirmed by IRC calculations. Further evidence comes from the transition vector of $TSOH(T_1)$ with the direction toward the formation of the radicals of $CH_3COCHCCH_3(\tilde{X}^2A)$ and $OH(\tilde{X}^2\Pi)$ in the ground state. The C2−O3 bond in $TSOH(T_1)$ is elongated to 2.050 Å, which is 0.681 Å longer than that in the E-T_1 minimum, and the C2−C7 bond length in $TSOH(T_1)$ is shortened to 1.370 Å from 1.490 Å in the E-T_1 minimum. The departure of the OH group leads to some double-bond character of the C2−C7 bond in $TSOH(T_1)$. With respect to the E-T_1 minimum, the barrier height of the C2−O3 bond fission on the E-$T_1(^3\pi\pi^*)$ potential energy surface was determined to be 46.8 kcal/mol at the CAS(10,8) level of theory.

The dissociation energy for the C2−O3 bond cleavage has been estimated to be 90.3 kcal/mol from the measured OH product state distributions.[48] The experimental value for the translational energy that is released into the OH photofragment is 16.0 kcal/mol,[49] which is assumed to be the exit barrier.[51] Thus, the position of $TSOH(T_1)$ in energy was experimentally inferred to be 106.3 kcal/mol above the E-S_0 minimum. With respect to the E-S_0 minimum, $TSOH(T_1)$ has its relative energy of 103.5 kcal/mol at the CAS(10,8) level of theory with the zero-point energy correction included. In comparison to the experimental value, the CAS(10,8) calculations gave a good description of the C2−O3 bond dissociation on the T_1 state. We attempted to optimize a transition state for C2−O3 bond scission from the E-$S_1(^1n\pi^*)$ state but were unsuccessful.

4. Mechanistic Aspects

Upon photoexcitation of $CH_3COCH_2COCH_3$ at 250 nm or shorter wavelengths, the enolic-AcAc molecule is located on the $S_2(^1\pi\pi^*)$ state. Experimentally, no fluorescence was observed from the $S_2(^1\pi\pi^*)$ state,[46,48] and the rate[49] of the OH radical formation is greater than 10^8 s^{-1}. This suggests that the $\pi \rightarrow \pi^*$ transition is followed by a very fast nonradiative decay process. As shown in Figure 1, the E-$S_2(^1\pi\pi^*)$ molecule adopts C_{2v} symmetry but E-$S_1(^1n\pi^*)$ has a planar structure. Once the H8 atom deviates from the center of the O3 and O11 atoms in the $S_2(^1\pi\pi^*)$ state this easily leads to the system in $S_1(^1n\pi^*)$ state. The normal modes are not only distorted but also mixed with each other in the $S_2 \rightarrow S_1$ relaxation process. The frequency change and mode mixing make the $S_2 \rightarrow S_1$ internal conversion (IC) occur with high efficiency through increasing the vibrational part of the IC rate constant.[60] Experimentally, it was observed that the energy difference between the S_2 and S_1 states is not large.[50,61] The present CAS(10,8) calculations predict the energy difference between the S_2 and S_1 minimum to be 21.7 kcal/mol. All the preceding evidence suggests that IC to the S_1 state from the S_2 state is the predominant ultrafast process responsible for depopulating S_2 following 250 nm excitation of S_0.

From the $S_1(^1n\pi^*)$ state, the enolic-AcAc molecule can relax via two nonradiative channels in addition to a radiation decay. They are IC to the ground state and intersystem crossing (ISC)

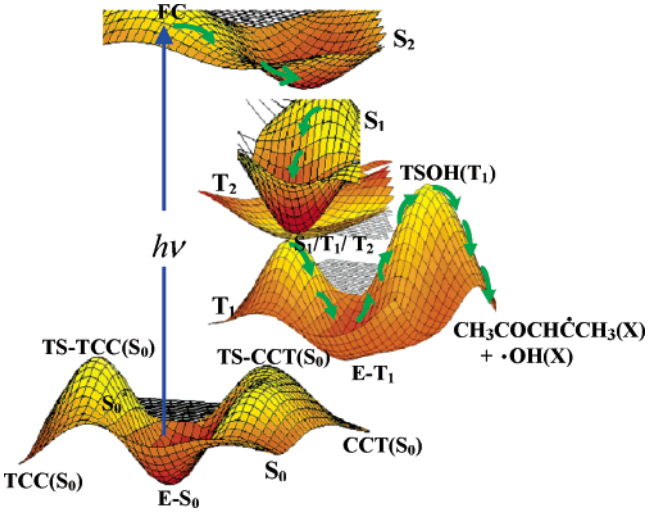

Figure 4. Schematic diagram of the most possible pathways upon photoexcitation of AcAc in the UV regions.

to the lower triplet state. The geometric structure for the S_1-($^1n\pi^*$), $T_2(^3n\pi^*)$ surface intersection has been optimized by searching for the lowest energy point of the two-surface crossing seam with the state-averaged CAS(10,8) calculations. Meanwhile, the intersection for the two lowest triplet states (T_1/T_2) was also determined with the state-averaged CAS(10,8) optimizations. When the geometric structures and energies of the S_1/T_2 and T_1/T_2 intersections were compared, it was found that there is little difference between the two intersections. Actually, the three surfaces (S_1, T_1, and T_2) intersect at the same region, and this triple curve crossing region is referred to as $S_1/T_1/T_2$ and is depicted in Figure 1. The $S_1/T_1/T_2$ intersection and the E-S_1 minimum have C_s symmetry structures. The C7−C10, C2−C7, and C10−O11 bond lengths are respectively 1.371, 1.439, and 1.352 Å in the $S_1/T_1/T_2$ structure. The corresponding values for these bond lengths are 1.386, 1.396, and 1.364 Å for the E-S_1 minimum. This indicates the $S_1/T_1/T_2$ intersection and the E-S_1 minimum are very close in structure. With respect to the E-S_1 minimum, the position of $S_1/T_1/T_2$ is only 0.5 kcal/mol higher in energy at the CAS(10,8) level of theory. The structural similarity and small energy gap between $S_1/T_1/T_2$ and E-S_1 indicates that ISC from $S_1(^1n\pi^*)$ to $T_1(^3\pi\pi^*)$ and then relaying on to $T_2(^3n\pi^*)$ may take place with a high probability. We failed to find the intersection of S_0 and $S_1(^1n\pi^*)$, and this suggests IC to the ground from the $S_1(^1n\pi^*)$ state probably occurs with much lower probability than the ISC process to the $T_1(^3\pi\pi^*)$ state.

In the $T_1(^3\pi\pi^*)$ state, the keto−enolic tautomerization takes place with little probability. The hydration reaction has a high barrier on the $T_1(^3\pi\pi^*)$ pathway. So, the predominant process in the $T_1(^3\pi\pi^*)$ state is the C2−O3 bond fission via the TSOH-(T_1) transition state. Certainly, it is also very possible that the enolic-AcAc molecule can consume a few kcal of energy to fulfill the energy needed for a rotation of O−H or CH_3COH to produce the isomer of CCT(T_1) or CTC(T_1) that subsequently undergoes C2−O3 scission.

5. Summary

The lowest five electronic states of S_0, T_1, T_2, S_1, and S_2 for enolic-AcAc have been determined by the CAS(10,8) computations. The S_0 and T_1 potential energy surfaces for photodissociation, rotational isomerization, and keto−enolic tautomerization have been mapped at the CAS(10,8) and B3LYP levels of theory. An overview perspective of the mechanism for the photochemistry of enolic-AcAc has been obtained based on the calculated potential energy surfaces and their intersection points. The enolic-AcAc molecule is initially promoted to the Franck−Condon (FC) region of the $S_2(^1\pi\pi^*)$ state by 250 nm excitation. Decay to the $S_1(^1n\pi^*)$ state takes place in a short period via a vibronic interaction, and finally it relaxes to the E-$T_1(^3\pi\pi^*)$ minimum through the $S_1/T_1/T_2$ three-surface intersection. Rotational isomerization proceeds easily on the $T_1(^3\pi\pi^*)$ state, and the six isomers may coexist. But the predominant decomposition process on the $T_1(^3\pi\pi^*)$ state is the C2−O3 cleavage, forming the fragments of $CH_3COCHCCH_3(\tilde{X}^2A)$ and $OH(\tilde{X}^2\Pi)$ in the ground state. These processes are summarized in Figure 4. Since rotational isomerization processes involve a breakage of the intramolecular O−H···O hydrogen bond or breaking the C=C π bond, these processes proceed difficultly in the ground state. The keto−enol tautomerization reaction does not take place for AcAc in the gas phase.

Acknowledgment. This work was supported by grants from the National Natural Science Foundation of China (Grant Nos. 20472011 and 20233020) and from the Major State Basic Research Development Programs (Grant Nos. 2004CB719903 and 2002CB613406).

Supporting Information Available: Structures and energies for all stationary points reported in the present work. This material is available free of charge via the Internet at http://pubs.acs.org.

References and Notes

(1) Hammond, G. S.; Borduin, W. G.; Guter, G. A. *J. Am. Chem. Soc.* **1959**, *81*, 4682−4686.
(2) Gordon, M. S.; Koob, R. D. *J. Am. Chem. Soc.* **1973**, *95*, 5863−5867.
(3) Holm, R. H.; Cotton, F. A. *J. Am. Chem. Soc.* **1958**, *80*, 5658−5663.
(4) Bock, B.; Flatau, K.; Junge, H.; Kuhr, M.; Musso, H. *Angew. Chem., Int. Ed. Engl.* **1971**, *10*, 225−235.
(5) Egan, W.; Gunnarsson, G.; Bull, T. E.; Forsen, S. *J. Am. Chem. Soc.* **1977**, *99*, 4568−4572.
(6) Cohen, B.; Weiss, S. *J. Phys. Chem.* **1984**, *88*, 3159−3162.
(7) Shapet'ko, N. N.; Bazov, V. P. *Zh. Fiz. Khim.* **1989**, *63*, 2832−2835.
(8) Gordon, M. S.; Koob, R. D. *J. Am. Chem. Soc.* **1973**, *95*, 5863−5867.
(9) Dannenberg, J. J.; Rios, R. *J. Phys. Chem.* **1994**, *98*, 6714−6718.
(10) Hinsen, K.; Roux, B. *J. Chem. Phys.* **1997**, *106*, 3567−3577.
(11) Buemi, G.; Gandolfo, C. *J. Chem. Soc., Faraday Trans. 2* **1989**, *85*, 215−227.
(12) Marvi, J.; Grdadolnik, J. *J. Phys. Chem.* **2001**, *105*, 2039−2044.
(13) Marvi, J.; Grdadolnik, J. *J. Phys. Chem.* **2001**, *105*, 2045−2051.
(14) Srinivasan, R.; Feenstra, J. S.; Park, S. T.; Xu, S.; Zewail, A. H. *J. Am. Chem. Soc.* **2004**, *126*, 2266−2267.
(15) Gilli, G.; Bellucci, F.; Ferretti, V.; Bertolasi, V. *J. Am. Chem. Soc.* **1989**, *111*, 1023−1028.
(16) Bertolasi, V.; Gilli, P.; Ferretti, V.; Gilli, G. *J. Am. Chem. Soc.* **1991**, *113*, 4917−4925.
(17) Dannenberg, J. J.; Rios, R. *J. Phys. Chem.* **1994**, *98*, 6714−6718.
(18) Gilli, P.; Bertolasi, V.; Ferretti, V.; Gilli, G. *J. Am. Chem. Soc.* **2000**, *122*, 10405−10417.
(19) Lowrey, A. H.; George, C.; Antoio, P. D.; Karle, J. *J. Am. Chem. Soc.* **1971**, *93*, 6399−6403.
(20) Rios, M. A.; Rodriguez, J. *THEOCHEM* **1990**, *63*, 137−144.
(21) Ishida, T.; Hirata, F.; Kato, S. *J. Chem. Phys.* **1999**, *110*, 3938−3945.
(22) Harris, R. K.; Rao, R. C. *Org. Magn. Reson.* **1983**, *21*, 580−586.
(23) Funck, E.; Mecke, R. In *Hydrogen Bonding*; Hadzi, D., Ed.; Pergamon Press: London, 1959; p 433.
(24) Cheng, L. T. Ph.D. Dissertation, Louisiana State University, Baton Rouge, LA, 1968.
(25) Houk, K. N.; Davis, L. P.; Newkomc, G. R.; Duke, R. E., Jr.; Nauman, R. V. *J. Am. Chem. Soc.* **1973**, *95*, 8364−8371.
(26) Powling, J.; Bernstein, H. J. *J. Am. Chem. Soc.* **1951**, *73*, 4353−4356.
(27) Spencer, J. N.; Holmboe, E. S.; Kirshenbaum, M. R.; Firth, D. W.; Pinto, P. B. *Can. J. Chem.* **1982**, *60*, 1178−1182.

(28) Emsley, J.; Freeman, N. J. *J. Mol. Struct.* **1987**, *161*, 193−204.
(29) Rogers, M. T.; Burdett, J. L. *Can. J. Chem.* **1965**, *43*, 1516−1526.
(30) Wallen, S. L.; Yonker, C. R.; Phelps, C. L.; Wai, C. M. *J. Chem. Soc., Faraday Trans.* **1997**, *93*, 2391−2394.
(31) Folkendt, M. M.; Weiss-Lopez, B. E.; Chauvel, J. P., Jr.; True, N. S. *J. Phys. Chem.* **1985**, *89*, 3347−3352.
(32) Nakanishi, H.; Morita, H.; Nagakura, S. *Bull. Chem. Soc. Jpn.* **1977**, *50*, 2255−2261.
(33) Schieringand, D. W.; Katon, J. E. *Appl. Spectrosc.* **1986**, *40*, 1049−1054.
(34) Bauer, S. H.; Wilcox, C. F. *Chem. Phys. Lett.* **1997**, *279*, 122−128.
(35) Mecke, R.; Funck, E. *Z. Elektrochem.* **1956**, *60*, 1124−1130.
(36) Lazaar, K. I.; Bauer, S. H. *J. Phys. Chem.* **1983**, *87*, 2411−2419.
(37) Folkend, M. M.; Weiss-Lopez, B. E.; Chuvel, J. P.; True, N. S. *J. Phys. Chem.* **1985**, *89*, 3347−3352.
(38) Ochterski, J. W.; Petersson, G. A.; Montgomery, J. A., Jr. *J. Chem. Phys.* **1996**, *104*, 2598−2619.
(39) Ishida, T.; Hirata, F.; Kato, S. *J. Chem. Phys.* **1999**, *110*, 3938−3954.
(40) Veierov, D.; Bercovici, T.; Fischer, E.; Mazur, Y.; Yogev, A. *J. Am. Chem. Soc.* **1973**, *95*, 8173−8175.
(41) Chiavassa, T.; Verlaque, P.; Pizzala, L.; Roubin, P. *Spectrochim. Acta, Part A* **1994**, *50*, 343−351.
(42) Roubin, P.; Chiavassa, T.; Verlaque, P.; Pizzala, L.; Bodot, H. *Chem. Phys. Lett.* **1990**, *175*, 655−659.
(43) Nagashima, N.; Kudoh, S.; Takayanagi, M.; Nakata, M. *J. Chem. Phys.* **2001**, *105*, 10832−10838.
(44) Coussan, S.; Manca, C.; Ferro, Y.; Roubin, P. *Chem. Phys. Lett.* **2003**, *370*, 118−125.
(45) Walzl, K. N.; Xavier, I. M., Jr.; Kuppermann, A. *J. Chem. Phys.* **1987**, *86*, 6701−6706.
(46) Yoon, M. C.; Choi, Y. S.; Kim, S. K. *Chem. Phys. Lett.* **1999**, *300*, 207−212.
(47) Yoon, M. C.; Choi, Y. S.; Kim, S. K. *J. Phys. Chem. A* **2000**, *104*, 4352−4355.
(48) Yoon, M. C.; Choi, Y. S.; Kim, S. K. *J. Chem. Phys.* **1999**, *110*, 11850−11855.
(49) Upadhyaya, H. P.; Kumar, A.; Naik, P. D. *J. Chem. Phys.* **2003**, *118*, 2590−2598.
(50) Xu, S.; Park, S. T.; Feenstra, J. S.; Srinivasan, R.; Zewail, A. H. *J. Phys. Chem.* **2004**, *108*, 6650−6655.
(51) North, S. W.; Blank, D. A.; Gezelter, J. D.; Longfellow, C. A.; Lee, Y. T. *J. Chem. Phys.* **1995**, *102*, 4447−4460.
(52) (a) Fang, W. H.; Phillips, D. L. *ChemPhysChem* **2002**, *3*, 889−892. (b) Fang, W.-H.; Liu, R.-Z.; Zheng, X.; Phillips, D. L. *J. Org. Chem.* **2002**, *67*, 8407−8415. (c) Chen, X.-B.; Fang, W. H. *J. Am. Chem. Soc.* **2003**, *125*, 9689−9698. (d) He, H.-Y.; Fang, W. H.; Phillips, D. L. *J. Phys. Chem. A* **2004**, *108*, 5386−5392. (e) Chen, X.-B.; Fang, W.-H. *J. Am. Chem. Soc.* **2004**, *126*, 8976−8980.
(53) Frisch, M. J.; Trucks, G. W.; Schlegel, H. B.; Scuseria, G. E.; Robb, M. A.; Cheeseman, J. R.; Zakrzewski, V. G.; Montgomery, J. A.; Stratmann, R. E.; Burant, J. C.; Dapprich, S.; Millam, J. M.; Daniels, A. D.; Kudin, K. N.; Strain, M. C.; Farkas, O.; Tomasi, J.; Barone, V.; Cossi, M.; Cammi, R.; Mennucci, B.; Promelli, C.; Adamo, C.; Clifford, S.; Ochterski, J.; Petersson, G. A.; Ayala, P. Y.; Cui, Q.; Morokuma, K.; Malick, D. K.; Rabuck, A. D.; Raghavachari, K.; Foresman, J. B.; Cioslowski, J.; Ortiz, J. V.; Stefanov, B. B.; Liu, G.; Liashenko, A.; Piskorz, P.; Komaromi, I.; Gomperts, R.; Martin, R. L.; Fox, D. J.; Keith, T.; Al-Laham, M. A.; Peng, C. Y.; Nanayakkara, A.; Gonzalez, C.; Challacombe, M.; Gill, P. M. W.; Johnson, B. G.; Chen, W.; Wong, M. W.; Andres, J. L.; Head-Gordon, M.; Replogle, E. S.; Pople, J. A. *Gaussian 98*; Gaussian, Inc.: Pittsburgh, PA, 1998.
(54) Iijima, K.; Ohnogi, A.; Shibata, S. *J. Mol. Struct.* **1987**, *156*, 111−118.
(55) Camerman, A.; Mastropaolo, D.; Camerman, N. *J. Am. Chem. Soc.* **1983**, *105*, 1584−1586.
(56) Boese, R.; Antipin, M. Y.; Bläser, D.; Lyssenko, K. A. *J. Phys. Chem. B* **1998**, *102*, 8654−8660.
(57) Andreassen, A. L.; Bauer, S. H. *J. Mol. Struct.* **1972**, *12*, 381−403.
(58) Hush, N. S.; Livett, M. K.; Peel, J. B.; Willett, G. D. *Aust. J. Chem.* **1987**, *40*, 599−609.
(59) Yamabe, S.; Tsuchida, N.; Miyajima, K. *J. Phys. Chem. A* **2004**, *108*, 2750−2757.
(60) Mebel, A. M.; Hayashi, M.; Liang, K. K.; Lin, S. H. *J. Phys. Chem. A* **1999**, *103*, 10674−10690 and references therein.
(61) Lim, E. C. *J. Phys. Chem.* **1986**, *90*, 6770−6777.